PREDICTIVE ANALYTICS OF CIGS SOLAR CELL USING A COMBINATIONAL GRA-MLR-GA MODEL

K. E. KAHARUDIN, F. SALEHUDDIN*,
A. S. M. ZAIN, AMEER F. ROSLAN

MiNE, CeTRI, Faculty of Electronics and Computer Engineering (FKEKK),
Universiti Teknikal Malaysia Melaka (UTeM), Hang Tuah Jaya,
Durian Tunggal, 76100 Melaka, Malaysia
*Corresponding Author: fauziyah@utem.edu.my

Abstract

Thin-film Copper Indium Gallium Selenide (CIGS) solar cell is identified to be one of the promising structures to replace conventional silicon-based solar cell due to its lower cost and reduced thickness. Nevertheless, the impact of layer thickness and doping concentration of a window layer - Zinc oxide (ZnO), a buffer layer - Cadmium sulfide (Cds) and an absorber layer (CIGS) needs to be intelligently controlled for more balanced CIGS solar cell performances. Thus, this paper proposes a newly predictive analytics using a combination of Grey relational analysis (GRA), multiple linear regressions (MLR) and genetic algorithm (GA) to optimize the CIGS solar cell parameters for better device performances. The CIGS solar cell model is developed and simulated using solar cell capacitance simulator (SCAPS). The final results prove that the proposed combinational GRA-MLR-GA model has successfully optimized the CIGS solar cell parameters in which ZnO thickness (T_{ZnO}), Cds thickness (T_{Cds}), CIGS thickness (T_{CIGS}) and CIGS doping concentration (Na_{CIGS}) are predictively optimized to be 0.03 μm, 0.03 μm, 2.86 μm and 9.937x10^{17} cm^{-3} respectively. The most optimum magnitudes for open circuit voltage (V_{oc}), short circuit current density (J_{sc}), fill factor (FF), and power conversion efficiency (η) after the predictive analytics are measured at 0.8206 V, 32.419 mA/cm^2, 83.23% and 22.14% reciprocally.

Keywords: Fill factor, Open circuit voltage, Power conversion efficiency, Short circuit current density.

1. Introduction

Multiple approaches to developing thin-film solar cells have tremendously received a lot of attention nowadays as they are believed to contribute significant improvements in solar cell efficiency. In addition, a thin-film of solar cell significantly eases the manufacturing process because the fabrication processes depend on multiple layer substances, hence not having to rely on the molten silicon that would probably take longer production time. One prominent advantage of thin-film solar cell is its direct band-gap energy where the lattice momentum of electrons and holes is equivalent in both conduction and valence band, subsequently allowing an electron to directly diffuse a photon.

Copper Indium Gallium Selenide (CIGS) solar cell is one of the popular types of thin-film photovoltaic devices that utilize GIGS layer to emulate as a p-type absorber material. At the moment, research and development on CIGS solar cell is still rapidly being conducted for better device performances and reduced cost. One of the effective methods to further improve CIGS solar cell performances is by controlling the random variation of material parameters. Numerous simulation attempts on improving the CIGS solar cell performances have been previously conducted [1-4] by optimizing the different material layer thickness and doping concentration. Thus, tuning both material thickness and doping concentration has been recognized as a practical approach to improve solar cell performances [5-8].

A lot of predictive optimization methods have been introduced and employed to improve multiple types of device and product properties [9-14]. The primary objective of these predictive optimization approaches (e.g., Taguchi method, response surface methodology, factorial design and etc.) is to identify the optimum magnitude of input parameters that would subsequently yield the best output performances [15-19]. Thus, this paper will introduce a newly predictive analytics using a combination of Grey relational analysis (GRA), multiple linear regression (MLR) and genetic algorithm (GA) to optimize the CIGS solar cell parameters for improved performances. The organization of this manuscript is defined as follows: Section 2 describes the numerical simulation of the CIGS solar cell using solar cell capacitance simulator (SCAPS). Section 3 generally explains the proposed predictive analytics using a combinational GRA-MLR-GA model. Section 4 comprehensively discusses the results of the predictive analysis. Finally, the conclusions of this present work are presented in Section 5.

2. Numerical Simulation

In the current work, numerical simulation and modeling of thin-film CIGS solar cell have been conducted using solar cell capacitance simulator (SCAPS). Originally, SCAPS is a freely available one-dimensional solar cell simulation software developed by the Department of Electronics and Information Systems (ELIS) of the University of Gent, Belgium [20]. SCAPS has been widely used in photovoltaic researches especially for investigating the impact of semiconductor layers with multiple defect levels upon the solar cell performance [21-23]. Furthermore, SCAPS allows multiple structures of the photovoltaic cell with different numbers and types of a layer to be simulated at multiple doping profiles (donor/acceptor) in accordance with a specific light spectrum.

The numerical simulation was initiated with three layers of CIGS model in which the baseline was configured with a Copper Indium Gallium Selenide (CIGS) layer as an absorber layer, stacked together with Cadmium Sulfide (Cds) as a buffer layer and Zinc Oxide (ZnO) as a window layer. The completed structure comprises window (ZnO) layer, buffer (Cds) layer, p-type absorber (CIGS) layer, back contact (Molybdenum) layer and glass substrate layer as illustrated in Fig. 1.
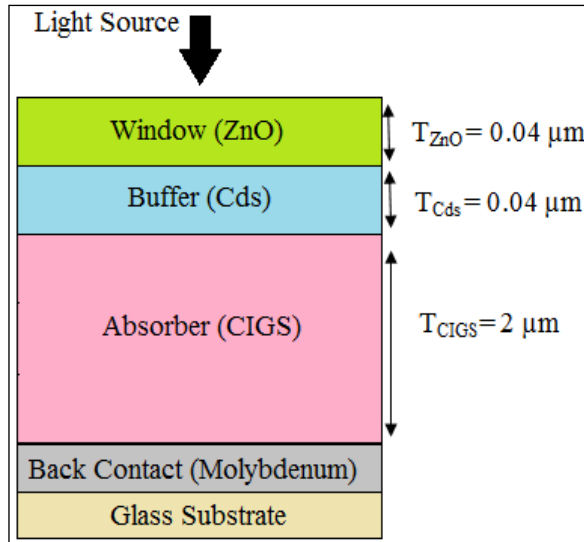

Fig. 1. Cross-sectional structure of CIGS solar cell.

Both window and buffer layers were initially set at 0.04 μm of thickness while the absorber layer was set at 2 μm of thickness. The thickness of the absorber layer is selected in a way that it must be greater than penetration depth of the longest wavelength absorbed. As for the window layer it must be capable enough to absorb the energetic photons and subsequently let them diffuse to the junction. The back contact (Molybdenum) and glass substrate were pre-defined in SCAPS software and their parameters would remain unchanged. The main function of the back contact was to reflect the unabsorbed sunlight back to the absorber for much better conversion efficiency. The bandgap energy (E_g) and the electron affinity, (E_{ea}) were fixed at 1.20 eV and 4.25 eV in conjunction with the previous reports in [1, 24] as tabulated in Table 1.

Table 1. Test model specifications and test conditions.

Parameter	p-CIGS	n-Cds	n-ZnO
Band gap, E_g (eV)	1.2	2.40	3.30
Electron affinity, E_{ea} (eV)	4.25	4.20	4.45

The simulations were carried out within the specified ranges of material parameters in each defined layer of the photovoltaic cell. The initial magnitude of the related parameters for ZnO, Cds and CIGS are within the reasonable ranges based on previous literatures [4, 6] as tabulated in Table 2. Device simulation was conducted under the illumination AM 1.5G in which the incident light power was set at 1000

W/m^2. The initial results are expressed in the current density-voltage (*J-V*) transfer characteristic as depicted in Fig. 2.

Table 2. Initial Magnitude of Material Parameters for CIGS Solar Cell.

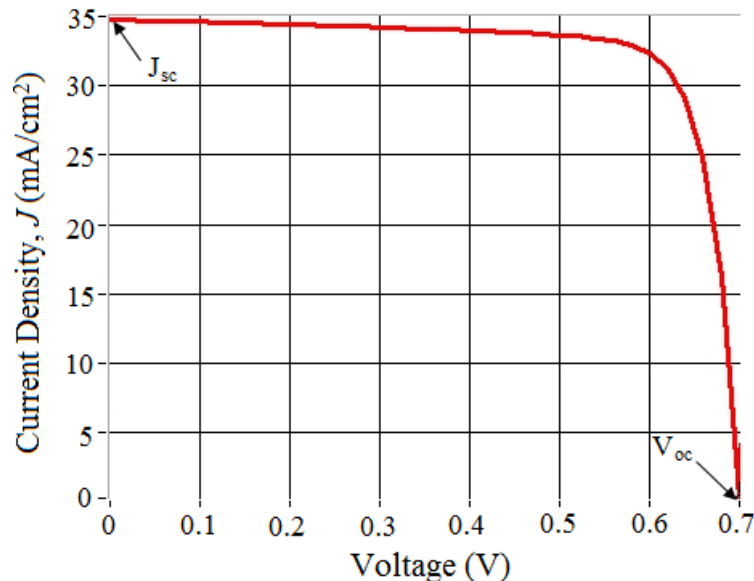| Material Parameters	Units	Magnitude
ZnO (Window) Thickness, T_{ZnO}	μm	0.04
CdS (Buffer) Thickness, T_{Cds}	μm	0.04
CIGS (Absorber) Thickness, T_{CIGS}	μm	2
CIGS (Absorber) Doping, Na_{CIGS}	cm^{-3}	1×10^{16}

Fig. 2. Initial *J-V* transfer characteristic of CIGS solar cell.

Based on Fig. 2, the initial magnitude for open-circuit voltage (V_{oc}) and short circuit current density (J_{sc}) are measured at 0.7002 V and 34.771 mA/cm^2. The V_{oc} is the maximum voltage of the CIGS solar cell measured at zero current while the J_{sc} is the current density that flows through the CIGS solar cell when the voltage is set to zero (short-circuited). Based on the measured magnitude of both V_{oc} and J_{sc}, the fill factor (*FF*) of the CIGS solar cell can be mathematically computed as:

$$FF = \frac{V_{mp} J_{mp}}{V_{oc} J_{sc}} \tag{1}$$

where V_{mp} and J_{mp} represents voltage and current density at maximum power point respectively. The *FF* is basically associated with the maximum power output in which a higher *FF* leads to a larger output power. Another significant output parameter of the CIGS solar cell is power conversion efficiency (η) which is commonly utilized for benchmarking one type of solar cell to another. Power conversion efficiency (η) of the CIGS solar cell can be defined as the ratio of the maximum output power to the incident light power as mathematically described as:

$$\eta = \frac{J_{sc} \times FF \times V_{oc}}{P_{in}} \tag{2}$$

where P_{in} represents the incident light power. Throughout the initial simulation, the magnitude for V_{oc}, J_{sc}, FF and η are recorded as listed in Table 3.

Table 3. Initial Magnitude of output Parameters for CIGS Solar Cell.

Output Parameter	Units	Magnitude
Open circuit Voltage, V_{oc}	V	0.7002
Short Circuit Current Density, J_{sc}	A/cm^2	34.771
Fill Factor, FF	%	79.95
Power Conversion Efficiency, η	%	19.47

In the next section, the investigated material parameters (T_{ZnO}, T_{Cds}, T_{CIGS} and Na_{CIGS}) will be predictively optimized for more balanced CIGS solar cell performances using a combinational GRA-MLR-GA model.

3. Predictive Analytics using A GRA-MLR-GA model

This section describes the detailed steps of the predictive analytics employed for simultaneous optimization of material parameters for more balanced in CIGS solar cell performances. The predictive analytics were initiated with the 18 sets of design of experiment (DoE) in which the material parameters as the independent variables were distributed into multiple levels (low, medium and high) as tabulated in Table 4.

The DoE was purposely constructed to retrieve sufficient data for developing the regression model in the subsequent stage. Each of the material parameters is symbolized with x_1, x_2, x_3 and x_4 respectively. All the 18 simulation runs were conducted based on the equally distributed DoE (Table 5) in order to attain adequate experimental data for predictive analytics. The magnitudes of multiple dependent variables (output parameters) for each experimental row are also recorded in Table 5.

Table 4. Independent inputs with multiple levels.

Symbols	Material Parameter	Unit	Level		
			Low	Medium	High
x_1	ZnO (Window) Thickness, T_{ZnO}	μm	0.03	0.04	0.05
x_2	CdS (Buffer) Thickness, T_{Cds}	μm	0.03	0.04	0.05
x_3	CIGS (Absorber) Thickness, T_{CIGS}	μm	1	2	3
x_4	CIGS (Absorber) Doping, Na_{CIGS}	cm^{-3}	1x10^{14}	1x10^{16}	1x10^{18}

The experimental data were then utilized and analysed using the predictive Grey Relational Analysis- Multiple Linear Regression (GRA-MLR-GA) model. Figure 3 depicts the overall process-flow of the predictive analytics using a combinational GRA-MLR-GA model.

Table 5. 18 sets of experimental design.

| Exp. no.	A	B	C	D	V_{oc} (V)	I_{sc} (mA/cm²)	FF (%)	η (%)
1	Low	Low	Low	Low	0.6946	35.272	82.92	20.32
2	Low	Low	Low	Medium	0.6984	34.674	80.46	19.48
3	Low	Low	Medium	High	0.813	31.599	83.46	21.44
4	Low	Medium	Medium	Low	0.6952	36.331	82.16	20.75
5	Low	Medium	High	Medium	0.7009	34.894	79.87	19.53
6	Low	Medium	High	High	0.821	32.376	82.76	22
7	Medium	High	Low	Low	0.6938	34.202	83.11	19.72
8	Medium	High	Low	Medium	0.6974	33.731	80.38	18.91
9	Medium	High	Medium	High	0.8116	31.267	85.52	20.94
10	Medium	Low	Medium	Low	0.6956	36.828	82.11	21.03
11	Medium	Low	High	Medium	0.7012	35.203	80.11	19.78
12	Medium	Low	High	High	0.8215	32.411	83.2	22.15
13	High	Medium	Low	Low	0.6941	34.572	83.05	19.93
14	High	Medium	Low	Medium	0.6978	34.149	80.26	19.12
15	High	Medium	Medium	High	0.8122	31.32	83.06	21.13
16	High	High	Medium	Low	0.6948	35.826	82.16	20.45
17	High	High	High	Medium	0.7004	34.286	80.04	19.22
18	High	High	High	High	0.82	32.081	82.32	21.66
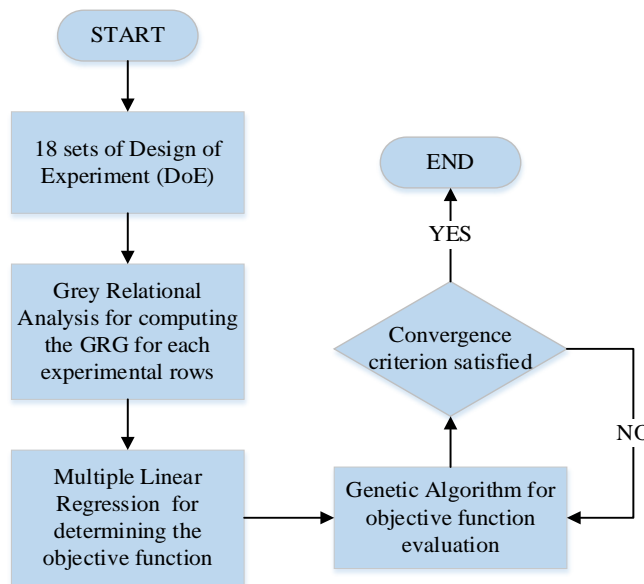
Fig. 3. Overall process-flow of the predictive analytics using a combinational GRA-MLR-GA model.

3.1. Grey relational analysis (GRA)

Grey relational analysis (GRA) is an effective approach to analyse any type of incomplete or uncertain information. The GRA was a part of grey system theory introduced by Deng Ju Long in 1982 [25] which capable of providing and

identifying robust solutions for real-world problems. This approach has been adopted in various field of engineering and solved multiple types of engineering problems. In this current study, the GRA is employed to convert multiple output parameters (V_{oc}, J_{sc}, FF and η) with different objective problems into a single representative unit called grey relational grade (GRG). The GRA requires several mathematical algorithms such as data normalization, deviation sequences, grey relational coefficients (GRC) and grey relational grades (GRG) as shown in Fig. 4.
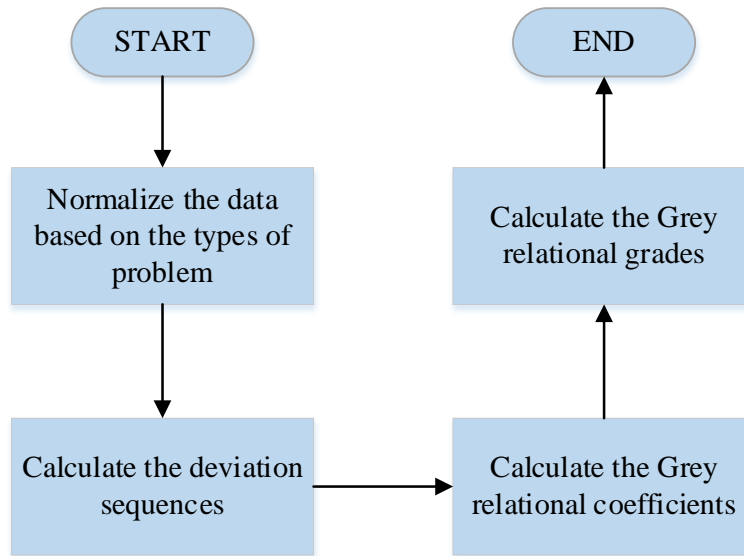

Fig. 4. Flowchart of the Mathematical Algorithms in GRA.

The GRA is basically adopted to convert the V_{oc}, J_{sc}, FF and η of the CIGS solar cell into a GRG with respect to their corresponding objective problems. In this case, all the investigated output parameters (V_{oc}, J_{sc}, FF and η) fall into a similar type of objective problem which is larger-the-better. Thus, the initial step in the GRA is to normalize all of the four output parameters by using Eqn. (2) [25] :

$$x_i^*(k) = \frac{x_i(k) - \min x_i(k)}{\max x_i(k) - \min x_i(k)} \tag{3}$$

where $x_i^*(k)$, $x_i(k)$, $\min x_i(k)$ and $\max x_i(k)$ are the sequence after data normalization, comparability sequence of the respective row, minimum sequence of the respective column and maximum sequence of the respective column accordingly. Based on the calculated $x_i^*(k)$, the deviation sequences, $\Delta_{oi}(k)$ can be determined as Eqn. (4):

$$\Delta_{oi}(k) = \left| x_0^*(k) - x_i^*(k) \right| \tag{4}$$

where $xo^*(k)$ is the reference sequence which is normally set to 1. From the calculated $\Delta_{oi}(k)$ for each experimental rows, the Grey relational coefficient (GRC), $\xi(k)$ for 18 experimental rows can be calculated using Eq. (5):

$$\xi(k) = \frac{\Delta_{\min} + \xi\Delta_{\max}}{\Delta_{oi}(k) + \xi\Delta_{\max}} \tag{5}$$

where ξ, Δ_{max} and Δ_{min} are an identification coefficient, a maximum absolute difference and a minimum absolute difference reciprocally. The magnitude of ξ is set to be 0.5 because of it brings balanced distinguishing effect and stability. In fact, the alteration in ξ will only change the magnitude of GRC but it will not affect the rank of the Grey relational grade (GRG). The magnitude of Δ_{max} and Δ_{min} is set to 1 and 0 respectively. Based on the calculated $\xi(k)$, the GRG for 18 experimental rows can be determined using:

$$\gamma_i = \frac{1}{4}\left[\xi_1 + \xi_2 + \xi_3 + \xi_4\right] \tag{6}$$

The GRG, γ_i for 18 experimental rows are basically computed by taking the average magnitude of the GRC, $\xi(k)$ of each experimental rows. In the next section, the calculated GRG, γ_i for 18 experimental rows will be further analysed using multiple linear regression (MLR) for deriving the objective function.

3.2. Multiple linear regression (MLR)

Multiple Regression Analysis (MLR) is a statistical method that utilizes multiple independent variables to estimate the outcome of a dependent variable. The prime objective of the MLR is to develop a linear model between independent variables (material parameters) and a dependent variable (GRG). In this study, MLR is employed to derive the objective function which will be further analysed using genetic algorithm (GA). In essence, the linear regression model for this study is relationally expressed as:

$$Y = b_0 + b_1 x_1 + b_2 x_2 + b_3 x_3 + b_4 x_4 + e \tag{7}$$

where $x_1 x_2 x_3 x_4$ are the material parameters, b_0 is the intercept, $b_1 b_2 b_3 b_4$ is the regression coefficients and e is the error term. Since the DoE consists of 18 experimental rows, the MLR equation can also be expressed in matrix form as:

$$\begin{pmatrix} y_1 \\ y_2 \\ \vdots \\ y_{18} \end{pmatrix} = \begin{pmatrix} x_{1,1} & x_{1,2} & x_{1,3} & x_{1,4} \\ x_{2,1} & x_{2,2} & x_{2,3} & x_{2,4} \\ \vdots & & & \\ x_{18,1} & x_{18,2} & x_{18,3} & x_{18,4} \end{pmatrix} \begin{pmatrix} b_o \\ b_1 \\ \vdots \\ b_{18} \end{pmatrix} + \begin{pmatrix} e_1 \\ e_2 \\ \vdots \\ e_{18} \end{pmatrix} \tag{8}$$

For the purpose of predicting the regression coefficients, the error terms are neglected in which the magnitude of b_0, b_1, b_2, b_3 and b_4 can be calculated by solving the matrices. Hence, the objective function of the current problem can be simply expressed as Eqn. (9):

$$Y^{'} = b_0 + b_1 x_1 + b_2 x_2 + b_3 x_3 + b_4 x_4 \tag{9}$$

3.3. Genetic algorithm (GA)

Genetic algorithm (GA) is invented based on the biological processes occurred in natural evolution. The prime objective of the GA is to fully utilize this systematic evolution to solve multiple objective problems. The fundamental principle of the GA is to simulate certain processes in natural systems required for evolution. In

this study, GA is predominantly employed to search a local optimum of the objective function which has been previously derived using MLR. Figure 5 shows the flowchart of the GA comprising multiple steps such as initial population, objective function, fitness scaling, selection, crossover and mutation.
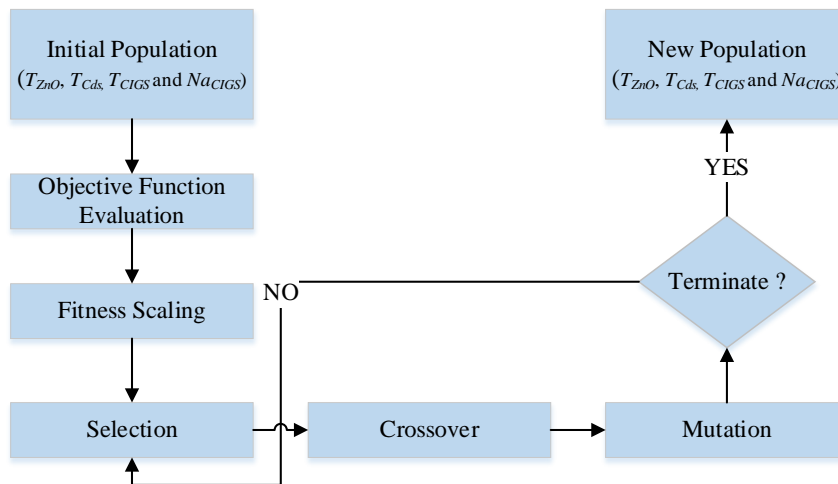

Fig. 5. Flowchart of the genetic algorithm.

Open source R-studio software has been utilized to aid in computing the GA optimization process. The initial population for this process is the initial magnitude of the T_{ZnO}, T_{Cds}, T_{CIGS} and Na_{CIGS} which have been listed in Table 4. Through MLR, the objective function of the problem has been identified and evaluated. Then, the objective function is fitly scaled within the specified upper and lower boundaries namely as the fitness function (f_i). The Rastringin function is selected as a test function to evaluate the optimization algorithm particularly in solving single-objective problem. It is commonly used for the problem that has multiple local minima formulated as:

$$Ras(x) = 10n + \sum_{i=1}^{n}\left[x_i^2 - 10\cos(2\pi x_i)\}\right] \tag{10}$$

where n is a total number of independent variables (material parameters) and x_i is the independent variable (GRG). The Rastringin function is evaluated based on the hypercube $xi \in [-5.12, 5.12]$ for all $I = 1, 2, 3$ and 4. Since this function is originally employed for searching the local minima, it is then converted in order to search the local maxima. Thus, the fitness function (f_i) for the maximization problem can be formulated as:

Minimize – $Ras(x_1, x_2, x_3, x_4)$
Subject to the constraints:
$0.03 \leq x_1 \leq 0.05$
$0.03 \leq x_2 \leq 0.05$
$1 \leq x_3 \leq 3$
$1 \times 10^{14} \leq x_4 \leq 1 \times 10^{18}$

Next, each of the individual solutions generated from the fitness function (f_i) are

selected based on their level of fitness. The crossover is then performed to form a new offspring by utilizing the genes from the parent chromosomes. The process of mutation needs to be executed in order to avoid overloading all the possible solutions in the population into local optima of the function. For a certain number of generations, the process of selection, crossover and mutation are iterated until no significant improvement in the fitness value. At this point, the best fitness value of the fitness function is identified in which the new populations (T_{ZnO}, T_{Cds}, T_{CIGS} and Na_{CIGS}) are optimally predicted. The GA options for this recent study are set as:

Type = real-valued
Population size = 50
Number of generations = 1000
Elitism = 2
Crossover probability = 0.8
Mutation probability = 0.1

4. Results and Discussion

The results of the predictive analytics in predicting the most optimum material parameters for balanced CIGS solar cell performances will be critically discussed in this section. The experimental data from Table 5 are normalized using (3) and the deviation sequences of each row are subsequently computed using (4) as recorded in Table 6. Based on the computed deviation sequences, the GRCs for each row are calculated using (5) and then averaged to determine the GRGs for each rows as listed in Table 7.

Table 6. Deviation Sequences.

Exp. No.	Deviation Sequence, $\Delta_{oi}(k)$			
	$\Delta_{oi}(V_{oc})$	$\Delta_{oi}(J_{sc})$	$\Delta_{oi}(FF)$	$\Delta_{oi}(\eta)$
1	0.993735	0.279806	0.460177	0.564815
2	0.963978	0.38734	0.895575	0.824074
3	0.066562	0.940299	0.364602	0.219136
4	0.989037	0.089372	0.59469	0.432099
5	0.944401	0.347779	1	0.808642
6	0.003915	0.800575	0.488496	0.046296
7	1	0.472217	0.426549	0.75
8	0.971809	0.556914	0.909735	1
9	0.077525	1	0	0.373457
10	0.985904	0	0.60354	0.345679
11	0.942052	0.292214	0.957522	0.731481
12	0	0.794282	0.410619	0
13	0.997651	0.405682	0.437168	0.685185
14	0.968677	0.481748	0.930973	0.935185
15	0.072827	0.990469	0.435398	0.314815
16	0.992169	0.180183	0.59469	0.524691
17	0.948316	0.457112	0.969912	0.904321
18	0.011746	0.853623	0.566372	0.151235

Table 7. GRCs and GRGs.

Exp. No.	GRC, $\xi_i(k)$				GRG (γ_i)	Rank
	$\xi_i(V_{oc})$	$\xi_i(J_{sc})$	$\xi_i(FF)$	$\xi_i(\eta)$		
1	0.3347	0.6411	0.5207	0.4695	0.4915	10
2	0.3415	0.5634	0.3582	0.3776	0.4102	15
3	0.8825	0.3471	0.5783	0.6952	0.6258	5
4	0.3357	0.8483	0.4567	0.5364	0.5443	8
5	0.3461	0.5897	0.3333	0.3820	0.4128	14
6	0.9922	0.3844	0.5058	0.9152	0.6994	2
7	0.3333	0.5142	0.5396	0.4	0.4468	12
8	0.3397	0.4730	0.3546	0.3333	0.3752	18
9	0.8657	0.3333	1	0.5724	0.6928	3
10	0.3364	1	0.4530	0.5912	0.5952	6
11	0.3467	0.6311	0.3430	0.4060	0.4317	13
12	1	0.3863	0.5490	1	0.7338	1
13	0.3338	0.5520	0.5335	0.4218	0.4603	11
14	0.3404	0.5092	0.3494	0.3483	0.3868	17
15	0.8728	0.3354	0.5345	0.6136	0.5891	7
16	0.3350	0.7350	0.4567	0.4879	0.5037	9
17	0.3452	0.5224	0.3401	0.3560	0.3909	16
18	0.9770	0.3693	0.4689	0.7677	0.6457	4

The correlation between the material parameters and the GRGs are then developed via MLR as graphically plotted in Fig. 6. The quantile-quantile (Q-Q) plot in Fig. 6 shows a set of data reasonably sourced from normal distribution. It is important to note that the reference line (straight line) is dependent on the scale GRGs and location of the theoretical distribution.
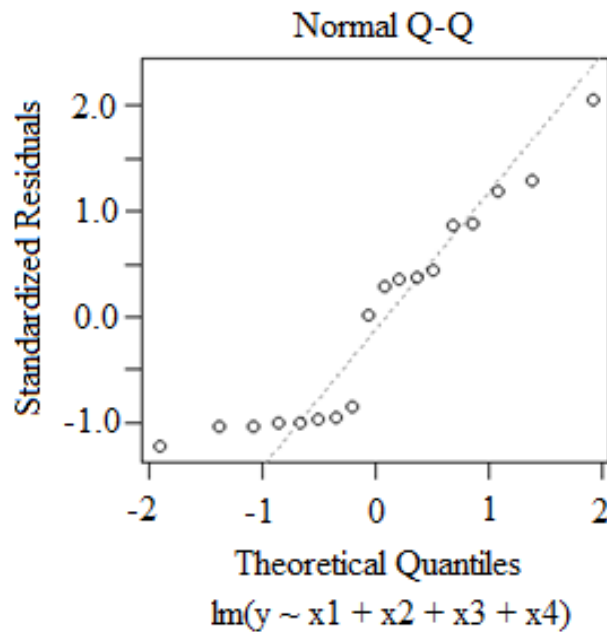

Fig. 6. Q-Q plots for GRGs.

The scattered points on the plot are observed to form a curve rather than a straight line implying the skewness in the computed GRGs. In this case, most of GRG points are scattered near the reference line, implying that the GRGs are reasonably consistent with normality. The summary of MLR analysis is shown in Table 7. It is observed that the material parameters that contribute to the most significant impact on GRG variations are x_1 (T_{ZnO}) and x_4 (Na_{CIGS}).

The objective function of the current problem can be relationally described based on the estimated regression coefficients in Table 8 as:

$$Y = 5.312e-01 - 1.001x_1 - 1.437x_2 + 1.150e-02x_3 + 2.019e-19x_4$$

Since the problem of this study is to find the maximum possible GRG, the objective function is then inverted within specific upper and lower boundaries. Thus, the fitness function (f_i) for this problem can be written as:

$$Y = -5.312e-01 + 1.001x_1 + 1.437x_2 - 1.150e-02x_3 - 2.019e-19x_4$$

The f_i is then fed into GA for optimization purpose. After 945 iterations, the most optimum fitness value is successfully identified as depicted in Fig. 7.

Table 8. ANOVA results of the multiple regression analysis.

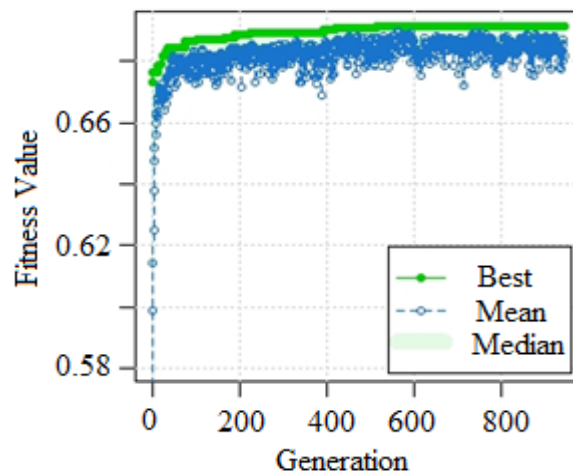| Term	Regression Coefficients	Std. Error	*t* value	*Pr* (>|*t*|)	Significant code
Intercept	5.312e-01	1.001e-01	5.309	0.00014	***
x1	-1.010	2.262	-0.447	0.66253	
x2	-1.437	2.262	-0.635	0.53619	
x3	1.150e-02	2.175e-02	0.529	0.60595	
x4	2.019e-19	3.787e-20	5.331	0.00014	***
Significant Code: 0 '***', 0.001 '**', 0.01 '*', 0.05 '.' 0.1-1 ' '					

Fig. 7. Performance of GA during convergence.

It is observed that the maximum fitness value (GRG) is measured at 0.6917469 in which the corresponding value of material parameters; T_{ZnO}, T_{Cds}, T_{CIGS} and Na_{CIGS}

are predicted to be 0.03 nm, 0.03 nm, 2.96 nm and 9.96 x 10^{17} cm^{-3} respectively. The CIGS solar cell is then re-simulated using the predicted value of material parameters for verification. Figure 8 shows the comparison of *J-V* transfer characteristic of CIGS solar cell before and after the proposed predictive analytics.
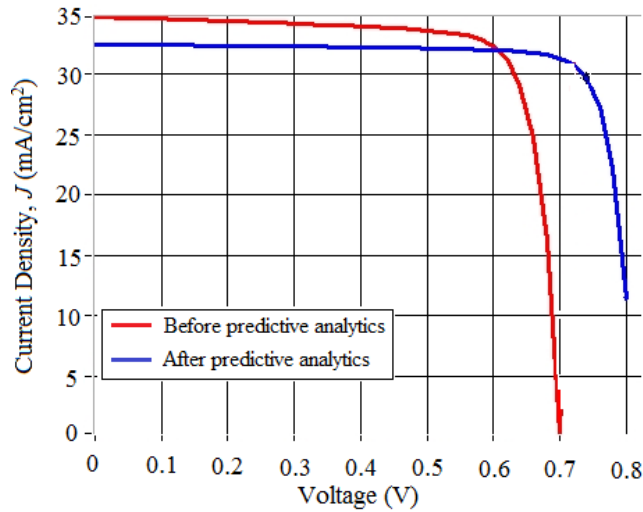

**Fig. 8. *J-V* transfer characteristic of CIGS
solar cell before and after predictive analytics.**

It is observed that the V_{oc} of the CIGS solar cell has been improved by ~14.7% after being optimized using the proposed predictive analytics. The V_{oc} of the CIGS solar cell is enhanced by employing much thicker absorber and buffer layers that boost the amount of voltage corresponding to the amount of forward bias caused by the light generated current when there is no current at the device junction. On the other hands, the J_{sc} of the device suffers a marginal decline for ~6.6% after being optimized using the proposed predictive analytics. This slight decline is mainly due to higher resistive loss caused by the random variations of the thickness of the absorber, window, CIGS layers and doping concentration. Nevertheless, both *FF* and *η* exhibits an improvement by ~3.9% and ~12.3% respectively as summarized in Table 9.

Table 9. Summary of the predictive analytics via GRA-MLR-GA model.

Output Parameters	Units	Before Predictive Analytics	After Predictive Analytics	% Differences
V_{oc}	V	0.7002	0.8213	~14.7%
J_{sc}	A/cm^2	34.771	32.473	~6.6%
FF	%	79.95	83.21	~3.9%
η	%	19.47	22.19	~12.3%

As the FF is closer to 1 (100%), more power can be generated by the CIGS solar cells under normal operating environment. Furthermore, higher power conversion efficiency (*η*) of the device is a very crucial parameter depending on the spectrum

and intensity of the incident sunlight and the temperature of the CIGS solar cell. The η of the device after predictive analytics is also compared to previous CIGS solar cell structures [1], [2, 6, 8], [26-29] for benchmarking purpose as depicted in Fig. 9.
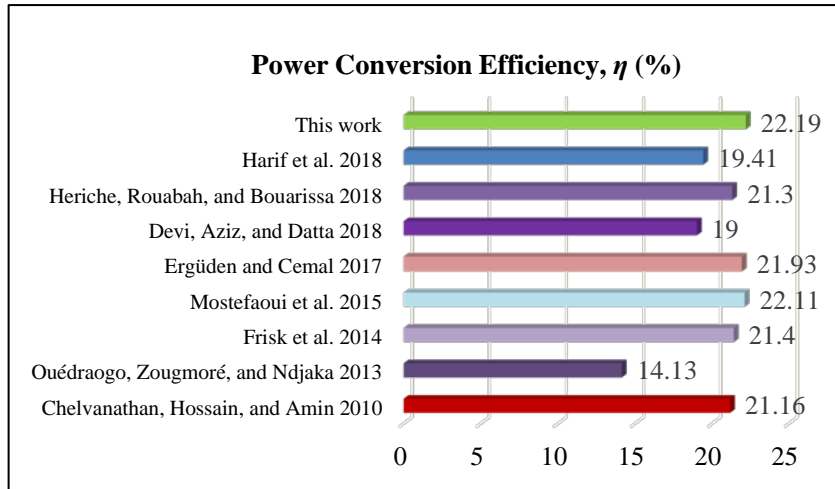

Fig. 9. Benchmark of power conversion
efficiency with previous CIGS solar cell structures.

The η of the CIGS solar cell after the predictive analytics (this study) has demonstrated the highest percentage among the others. This is predominantly due to the application of the proposed predictive analytics aiding in searching the possible optimum material parameters that could yield the most balanced output properties. Based on the comparative results, it is concluded that the predictive analytics using a combinational GRA-MLR-GA model can be regarded as a practical approach to optimize the material parameters of the CIGS solar cell in attaining holistically better cell performances. In future works, more material parameters including temperature, doping concentration and material types can be included in the proposed model for better robust solutions

5. Conclusions

In conclusion, a combinational model of Grey Relational Analysis (GRA), Multiple Linear Regression (MLR) and Genetic Algorithm (GA) are employed a predictive analytics to optimize the material parameters (T_{ZnO}, T_{Cds}, T_{CIGS} and Na_{CIGS}) in attaining holistically better CIGS solar cell performances. The initial step of this approach is to conduct the DoE with 18 experimental rows in order to retrieve the data for output parameters (V_{oc}, J_{sc}, FF and η). Afterwards, the corresponding data for V_{oc}, J_{sc}, FF and η in each row are converted into a single unit called GRG. The objective function that correlates between material parameters and GRG is then derived by using the MLR. The GA is subsequently used to fit the objective function within the upper and lower boundaries as a function of Rastringin called the fitness function (f_i). After having 945 iterative process cycles of selection, crossover and mutation, the most optimum fitness value (f_i) is identified at 0.6917469. As a result, the proposed combination model of GRA-MLR-GA has successfully predicted the best value of T_{ZnO}, T_{Cds}, T_{CIGS}, Na_{CIGS}, V_{oc}, J_{sc}, FF and η of the CIGS solar cell which are 0.03 nm,

0.03 nm, 2.96 nm, 9.96 x 10^{17} cm^{-3}, 0.8213 V, 32.473 A/cm^2, 83.21% and 22.19% respectively. Hence, it is concluded that the proposed predictive analytics using a combinational GRA-MLR-GA model could be possibly one of the effective approaches to optimize multiple material parameters of the CIGS solar cell for holistically better device performances.

Nomenclatures

E_{ea}	Electron affinity
E_g	Bandgap energy
e	Error term
fi	Fitness function
J_{mp}	Current density at maximum power point
J_{sc}	Short circuit current density
P_{in}	Incident light power
n	Total number of independent variables
V_{mp}	Voltage at maximum power point
V_{oc}	Open circuit voltage
$x_i^*(k)$	Sequence after data normalization
$x_i(k)$	Comparability sequence of the respective row
$xo^*(k)$	Reference sequence

Greek Symbols

$\Delta_{oi}(k)$	Deviation sequences
Δ_{max}	Maximum absolute difference
Δ_{min}	Minimum absolute difference
ξ	Identification coefficient
$\xi(k)$	Grey relational coefficient
γ_i	Grey relational grade
η	Efficiency

Abbreviations

Cds	Cadmium Sulfide
CIGS	Copper Indium Gallium Selenide
DoE	Design of Experiment
FF	Fill Factor
GA	Genetic Algorithm
GRA	Grey Relational Analysis
GRC	Grey Relational Coefficient
GRG	Grey Relational Grade
MLR	Multiple Linear Regression
Na$_{CIGS}$	CIGS Doping Concentration
RSM	Response Surface Methodology
SCAPS	Solar Cell Capacitance Simulator
T$_{Cds}$	Cds Thickness
T$_{CIGS}$	CIGS Thickness
T$_{ZnO}$	ZnO Thickness
ZnO	Zinc Oxide

References

1. Harif, M.N.; Abdullah, S.F.; Zuhdi, A.W.M.; Za'abar, F.; Bahrudin, M.S.; and Hasani, A.H. (2018). Simulation Analysis on CIGS Solar Cell On Different Absorber Layer Thickness Subject to Temperature Change Using SCAPS 1-D Software. *2018 IEEE International Conference on Semiconductor Electronics (ICSE)*, Kuala Lumpur, Malaysia, 201-204.

2. Mostefaoui, M.; Mazari, H.; Khelifi, S.; Bouraiou, A.; and Dabou, R. (2015). Simulation of High Efficiency CIGS Solar Cells with SCAPS-1D Software. *Energy Procedia*, 74, 736-744.

3. Tassoult, H.; and Bouloufa, A. (2014). The performance of SnO_2/CdS/CdTe type solar cell under influence of CdS buffer layer thickness and series resistance Rs, *Recent Advances in Biomedical & Chemical Engineering and Materials Science*, 134-137.

4. Heriche, H.; Rouabah, Z.; and Bouarissa, N. (2018). High-efficiency CIGS solar cells with optimization of layers thickness and doping Optik High-efficiency CIGS solar cells with optimization of layers thickness and doping. *Optik - International Journal for Light and Electron Optics*, 127(24), 11751-11757.

5. Alzoubi, T.; and Moustafa, M. (2019). Numerical optimization of absorber and CdS buffer layers in CIGS solar cells using SCAPS. *International Journal of Smart Grid and Clean Energy*, 8(3), 291-298.

6. Heriche, H.; Rouabah, Z.; and Bouarissa, N. (2018). New ultrathin CIGS structure solar cells using SCAPS simulation program. *International Journal of Hydrogen Energy*, 42(15), 9524-9532.

7. Freni, M.; Passalacqua. R.; Perathoner, S.; Centi, G.; Cannilla, C.; and Frusteri, F. (2015). Development of low-cost PV devices by using nanocrystal ink of light-absorbing CIGS semiconductor layer. *Chemical Engineering Transactions*, 43, 697-702.

8. Ergüden, S.A.; and Cemal, T. (2017). The Effect of Several Parameters on the Performance of CuInS2-based Solar Cells using SCAPS-1D Software. *Journal of Fundamental and Applied Sciences*, 68(3), 391-404.

9. Kaharudin, K.E; Salehuddin, F.; Zain, A.S.M.; and Aziz, M.N.I.A. (2017). Application of Taguchi-based Grey Fuzzy Logic for Simultaneous Optimization in TiO_2/WSi_x-based Vertical double-gate MOSFET. *Journal of Telecommunication, Electronic and Computer Engineering*, 9(2-13), 23-28.

10. Kaharudin, K.E; Salehuddin, F.; and Zain, A.S.M. (2018). Optimization of Electrical Properties in TiO_2/WSi_x-based Vertical DG-MOSFET using Taguchi-based GRA with ANN. *Journal of Telecommunication, Electronic and Computer Engineering*, 10(1), 69-76.

11. Kaharudin, K.E; Salehuddin, F.; Zain, A.S.M.; Aziz, M.N.I.A.; and Ahmad, I. (2016). Application of Taguchi Method with the Interaction Test for Lower DIBL in WSi_x/TiO_2 Channel Vertical Double Gate NMOS. *ARPN Journal of Engineering and Applied Sciences*, 11(11), 7093-7103.

12. Tripathy, S.; and Tripathy, D.K. (2017). Grey relational analysis and its application on surface properties during EDM and powder mixed EDM. *Journal of Engineering Science and Technology* (*JESTEC*), 12(9), 2374-2392.

13. Kaharudin, K.E; Salehuddin, F.; Zain, A.S.M.; Aziz, M.N.I.A.; and Ahmad, I. (2016). Optimization of process parameter variations on Threshold Voltage in Ultrathin Pillar Vertical Double Gate MOSFET Device. *ARPN Journal of Engineering and Applied Sciences*, 11(6), 3838-3848.

14. Kaharudin, K.E; Salehuddin, F.; Zain, A.S.M.; and Aziz, M.N.I.A. (2016). Taguchi Modeling with the Interaction Test for Higher Drive Current in WSI$_x$/TIO$_2$ Channel Vertical Double Gate NMOS Device. *Journal of Theoretical and Applied Information Technology*, 90(1), 185-193.

15. Tarasasanka, C.; and Ravindra, K. (2017). Application of Taguchi techniques to study dry sliding wear behaviour of magnesium matrix composites reinforced with alumina nano particles. *Journal of Engineering Science and Technology* (*JESTEC*), 12(11), 2855-2865.

16. Irawan, Y.S.; and Argo, B.D. (2017). Optimization of patchouli oil (Pogostemon cablin, benth) with steam distillation assisted by pulsed electric field via response surface methodology. *Journal of Engineering Science and Technology* (*JESTEC*), 12(8), 2106-2119.

17. Farahin Abdul Rahman, N.; Harun, S.; Sajab, M.S.; Zubairi, S.I., Markom, M.; Md Jahim, J.; Tusirin Mohd Nor, M.; Amrin Abdullah, M.; and Hashim, N. (2018). Boosting enzymatic hydrolysis of pressurized ammonium hydroxide pretreated empty fruit bunch using response surface methodology. *Journal of Engineering Science and Technology* (*JESTEC*), 13(8), 2421-2445.

18. Salehuddin, F.; Roslan, A.F.; Zailan, A.E.; Kaharudin, K.E.; Zain, A.S.M.; Afifah Maheran, A.H., Hanim, A.R.; Hazura, H.; Idris, S.K.; and Saad, W.H.M. (2018). Analyze of Process Parameter Variance in 19nm WSi2/TiO2 NMOS Device Using 2k-Factorial Design. *Journal of Telecommunication, Electronic and Computer Engineering*, 10(2), 127-131.

19. Kaharudin, K.E; Salehuddin, F.; Zain, A.S.M.; and Aziz, M.N.I.A. (2017). Comparison of Taguchi Method and Central Composite Design for Optimizing Process Parameters in Vertical Double Gate MOSFET. *ARPN Journal of Engineering and Applied Sciences*, 12(19), 5578-5590.

20. Niemegeers, A.; and Burgelman, M. (1996). Modelling of AC-Characteristics of Solar Cells. *Proceedings of the 25th IEEE Photovoltaic Specialists Conference*, Washington DC, USA, 901-904.

21. Burgelman, M.; Decock, K.; Kheli, S.; and Abass, A. (2013). Advanced electrical simulation of thin film solar cells. *Thin Solid Films*, 535, 296-301.

22. Decock, K.; Zabierowski, P.; Burgelman, M. (2012). Modeling metastabilities in chalcopyrite-based thin film solar cells Modeling metastabilities in chalcopyrite-based thin film solar cells. *Journal of Applied Physics*, 111(043703), 1-7.

23. Decock, K.; Zabierowski, P.; Burgelman, M. (2011). Modelling multivalent defects in thin film solar cells. *Thin Solid Films*, 519, 7481-7484.

24. Dejene, F.B.Ã. (2009). Solar Energy Materials & Solar Cells The structural and material properties of CuInSe$_2$ and Cu (In,Ga)Se$_2$ prepared by selenization of stacks of metal and compound precursors by Se vapor for solar cell applications. *Solar Energy Materials & Solar Cells*, 93, 577-582.

25. Ju-Long, D. (1982). Control problems of grey systems. *Systems and Control Letters*, 1(5), 288-294.

26. Chelvanathan, P.; Hossain, M. I.; Amin, N. (2010). Performance analysis of copper-indium-gallium-diselenide (CIGS) solar cells with various buffer layers by SCAPS. *Current Applied Physics*, 10, 387-391.

27. Ouédraogo, S.; Zougmoré, F.; Ndjaka, M. (2013). Numerical analysis of copper-indium-gallium-diselenide-based solar cells by SCAPS-1D. *International Journal of Photoenergy*, 2013, 1-9.

28. Frisk, C.; Platzer-Björkman, C.; Olsson, J.; Szaniawski, P.; Wätjen, J. T.; Fjällström, V.; Salomé, P.; Edoff, M. (2014). Optimizing Ga-profiles for highly efficient Cu (In, Ga) Se2 thin film solar cells in simple and complex defect models. *Journal of Physics D: Applied Physics*, 47(48), 1-12.

29. Devi, N.; Aziz, A.; Datta, S. (2018). Numerical modelling of CIGS/CdS solar cell. *AIP Conference Proceedings*, 1953, 1-6.